NANO MICRO small

Continuous Coaxial Electrohydrodynamic Atomization System for Water-Stable Wrapping of Magnetic Nanoparticles

*Sang-Yoon Kim, Jaemoon Yang, Bongjune Kim, Jungmin Park, Jin-Suck Suh, Yong-Min Huh, Seungjoo Haam, and Jungho Hwang**

An electrohydrodynamic atomization (EHDA) system that generates an electrospray can achieve particle formation and encapsulation by accumulating an electric charge on liquid flowing out from the nozzle. A novel coaxial EHDA system for continuous fabrication of water-stable magnetic nanoparticles (MNPs) is established, based on a cone-jet mode of electrospraying. Systemic variables, such as flow rates from dual nozzles and inducing voltages, are controlled to enable the preparation of water-soluble MNPs coated by polysorbate 80. The PEGylated MNPs exhibit water stability. The magnetic resonance imaging potential of these MNPs is confirmed by in vivo imaging using a gastric cancer xenograft mouse model. Thus, this advanced coaxial EHDA system demonstrates remarkable capabilities for the continuous encapsulation of MNPs to render them water-stable while preserving their properties as imaging agents.

1. Introduction

Magnetic nanoparticles (MNPs) have attracted a great deal of attention due to their unique properties and their potential applications in many fields. MNPs are emerging especially as promising candidates for drug delivery and biomedical imaging applications because of their ultrafine sizes, biocompatibility, and superparamagnetic properties.[1,2] High-resolution molecular and cellular imaging is one of the most promising applications of MNPs. Recently, MNPs were found to be excellent magnetic resonance (MR) imaging probes for noninvasive in vivo monitoring of molecular and cellular events.[3,4]

However, two common problems arise when applying these MNPs for in vivo MR imaging.[1,5,6] First, the MNPs become destabilized due to the adsorption of plasma proteins.

S.-Y. Kim,[+] Prof. J. Hwang
Department of Mechanical Engineering
Yonsei University
Seoul 120-749, Republic of Korea
E-mail: hwangjh@yonsei.ac.kr
Prof. J. Yang, J. Park, Prof. Y.-M. Huh
Department of Radiology
Yonsei University
Seoul 120-752, Republic of Korea
Prof. J. Yang
Severance Integrative Research Institute for Cerebral & Cardiovascular Diseases
Yonsei University Health System
Seoul 120-752, Republic of Korea
Prof. J. Yang, Prof. J.-S. Suh, Prof. Y.-M. Huh, Prof. S. Haam
YUHS-KRIBB Medical Convergence Research Institute
Seoul 120-752, Republic of Korea
B. Kim, Prof. S. Haam
Department of Chemical and Biomolecular Engineering
Yonsei University
Seoul 120-749, Republic of Korea
Prof. J.-S. Suh, Prof. Y.-M. Huh
Severance Biomedical Science Institute (SBSI)
Seoul 120-752, Republic of Korea
[+] These authors contributed equally to this work.

DOI: 10.1002/smll.201201553

Second, the MNPs are cleared nonspecifically by cells of the reticuloendothelial system (RES), such as macrophages.[7] Due to their large surface area, when exposed to a physiological environment the MNPs tend to interact with plasma proteins, which increases their size and often results in significant agglomeration of MNPs. MNPs are also recognized as foreign by the innate immune system and can be readily engulfed by macrophages. For both problems, MNPs are removed from the blood circulation system and lose their function quickly, thus leading to a dramatic reduction in the efficiency of nanoparticle-based diagnostics and therapeutics.

These problems can be circumvented by coating surfactants on MNPs. The surfactant coating serves as a protective layer and minimizes the direct exposure of the MNPs to the biological environment. Additionally, the coating can improve the stabilization of the MNPs in an aqueous phase. Generally, MNPs synthesized by thermal decomposition in the organic phase are considered to be the most suitable material because of their high magnetic sensitivity, low toxicity, and monodispersity in size.[8,9] These MNPs have oleic acid groups on their surface. The oleic acid groups are hydrophobic ligands, which can further increase the likelihood of interactions with plasma proteins. Moreover, due to their low colloidal stability in the aqueous phase, surface modifications are often required to increase the physicochemical stability of the MNPs.[10] Therefore, MNPs in organic solvents are usually coated with a surfactant for preparation of a stable aqueous magnetic solution.

PEGylation (polyethylene glycosylation) is one of the hydrophilic coating processes used to accomplish phase transfer of MNPs from the organic solvent phase to the aqueous phase. PEGylation can minimize the biofouling and aggregation of MNPs in physiological conditions due to the hydrophilicity and steric repulsion of PEG chains.[9,11–14] To date, several different anchor groups, including phosphate,[13] carboxylate,[15] silane,[12] and dopamine and its derivatives,[7,11] have been used to link PEG to the surface of MNPs. The anchor groups with high binding affinity can introduce a high-density PEG coating to improve stability.[16] The increased surface density of PEG improves the antibiofouling ability.[17] In fact, theoretical and experimental studies have demonstrated that, above a critical PEG surface density, the nonspecific adsorption of proteins to a substrate can be completely prevented.[18,19] During typical PEGylation, the MNPs are first synthesized and are then subjected to the surfactant solution under agitation.[20] However, as a batch process, PEGylation to produce stable MNPs in the aqueous phase is mass-limited.

A promising technique to generate a continuous surface coating is electrohydrodynamic atomization (EHDA), also referred to as electrospraying. In EHDA, a high-strength electric field induces accumulation of electric charge on the liquid flowing out from the nozzle, which leads to elongation of the liquid along the electric field. The mode of EHDA normally changes from a dripping mode to a cone-jet mode as the field strength increases. Overly high voltage makes the liquid unstable and generates a multijet mode. The cone-jet mode is desirable for the production of stable droplets with uniform size.[21,22] The generation of uniform-sized droplets in the EHDA process is possible only within a limited range of voltage and flow rate. Using this basic principle, a coaxial nozzle has great potential for forming coated droplets. A coaxial nozzle comprises two needles, one within the other. Two separate liquids can be forced through the nozzle, one through the inner needle and one through the annular space between the inner needle and the outer needle. Under suitable conditions, when the flow rate of the outer liquid is higher than that of the inner liquid and an appropriate voltage is set between the nozzle and ground electrode, the cone-jet will be composed of the inner liquid surrounded by the outer liquid.[23] The coaxial jet is subsequently broken up to form droplets of inner liquid surrounded by a coating layer of outer liquid. The final encapsulated droplet size can be on a micro- or nanoscale.[22] The key benefit of EHDA is that very fine droplets (usually from tens of nanometers to a few micrometers in diameter) can be obtained using relatively large nozzle sizes (several hundred micrometers in diameter).[24,25] This approach has been extensively studied for polymerization of core/shell structures,[22,23] composite ceramic structures,[26] coating drugs,[27,28] forming oil-in-water and oil-in-water-in-oil emulsions,[29,30] and building multilayered structures.[31] In all of these cases, the coated particles were larger than 100 nm.

Herein, we use a coaxial nozzle to synthesize an aqueous dispersion of monodispersed MNPs based on the EHDA process. To our knowledge, this is the first use of this technique to produce such MNPs. We also investigate the operating flow rate and applied voltage required to generate the stable coaxial jet. In this jet, the outer liquid (polysorbate) permeates into the inner liquid (hexane). Simultaneously, the inner liquid, which carries the MNPs, evaporates, which further differentiates our approach from existing methods that require two or more steps to achieve the hydrophilic coated MNPs. Following break-up of the stable coaxial jet, the monodispersed, polysorbate 80-coated MNPs fall into a distilled (DI) water bath and are stirred to complete the synthesis of the aqueous dispersion of MNPs. Finally, we demonstrate the MR imaging potential of the MNPs using an in vivo mouse model.

2. Results and Discussion

To prepare water-stable MNPs by the coaxial EHDA system, monodispersed MNPs (Fe_3O_4, 8.2 nm) were synthesized by thermal decomposition and seed-mediated growth. The prepared MNPs (30 mg) were dissolved in hexane (10 mL) and coated by oleic acids during the thermal decomposition process. The coaxial EHDA system consisted of a liquid supply system, a stirring system, a visual system, and an electrical system, as shown in **Figure 1**a. The organic solvent (hexane) containing MNPs was injected into the inner needle by a syringe pump, as shown in Figure 1b. Polysorbate 80 (commercially known as Tween 80), a viscous, yellow, nonionic surfactant, was used to suspend the MNPs in an aqueous phase. The surfactant was injected into the outer needle by another syringe pump. The surfactant-coated MNPs were dispersed in DI water. **Table 1** shows the properties of MNPs

NANO MICRO small

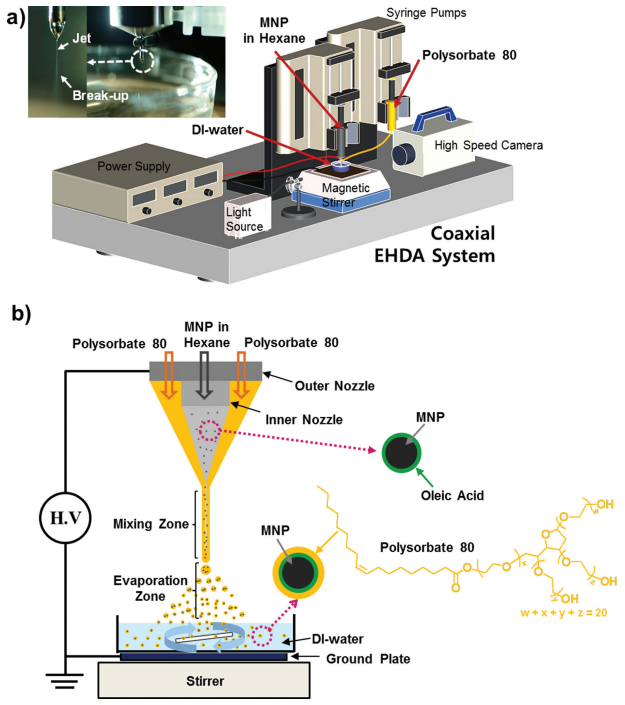

Figure 1. a) Schematic illustration of the coaxial EHDA system and b) the fabrication procedure of water-stable MNPs (polysorbate 80-coated MNPs) in an aqueous phase.

Table 1. Properties of water-stable MNPs suspended in hexane and polysorbate 80.

Property	Density [kg m^{-3}]	Viscosity [mPa s]	Surface tension [dyne cm^{-1}]	Electrical conductivity [μS cm^{-1}]
inner liquid (hexane with MNPs)	513	0.6	19.9	0.1
outer liquid (polysorbate 80)	1060	402	38.7	0.0068

suspended in hexane and polysorbate 80. Density was determined from the mass and volume of the liquids. Viscosity was measured with a vibration viscometer. The surfactant had greater density, viscosity, and surface tension than the hexane. The viscosity of the outer liquid was sufficiently high to diffuse the electrical stresses acting on the outer surface into the bulk, which resulted in the stable cone-jet mode.

To find an operating range of parameters for stable cone-jet formation, various inner and outer flow rates were tested with increasing applied voltage (**Figure 2**). When the flow rate to the inner nozzle was fixed as 10 μL min^{-1}, the flow rate to the outer nozzle was varied from 10 to 50 μL min^{-1}. To obtain a stable cone-jet, the electrohydrodynamic (EHD) forces must act on at least one liquid, although they may act on both. Accordingly, the applied voltage was first tuned for only the inner liquid, and then tuned for both liquids, to achieve the appropriate EHD forces to maintain a cone-jet. Figure 2a shows photos of various EHDA modes that were observed with high-speed video at different applied voltages, including dripping, microdripping, cone-jet, and multijet modes. Figure 2b summarizes the relationship between the various EHDA modes and the applied voltage. Extended pendants, which indicate a dripping mode, were observed at voltages less than 6.6 kV for single-nozzle flow and 7.3 kV for dual-nozzle flow. In the dripping mode, the meniscus was not transformed into a cone shape, and the generated droplets were larger than the nozzle diameter. Microdripping was observed at 7.6 kV for single-nozzle flow and 8.3 kV for dual-nozzle flow. At about 7.7 kV for the single nozzle and 8.7 kV for the dual nozzles, a stable cone-jet formed. However, when the voltage reached 11.0 kV for the single nozzle and 11.6 kV for the dual nozzles, the flow transformed to a multijet mode. Following this tuning, the applied voltage was fixed at 9 kV, which preserved the cone-jet mode for both single and dual nozzle configurations. At these settings, water-stable, polysorbate 80-coated MNPs were formed following the jet break-up (see Figure 1a). Aqueous dispersions of MNPs were synthesized by operating in the cone-jet mode for 1 h.

A number of particle size measurements were performed. Polysorbate 80-coated MNPs exhibited a size of almost 1 μm near the outlet of the coaxial nozzles (measured with an aerodynamic particle sizer (APS); **Figure 3**a, lower), which is much larger than the size of the MNPs (8.2 nm). The atomized droplets had a total concentration of 1.03×10^3 MNPs cm^{-3}, a geometric mean diameter of 1.11 μm, and a geometric standard deviation of 1.42. However, after they passed through the evaporation zone, the size decreased an order of magnitude (see Figure S1 in the Supporting Information) as the hexane evaporated, and exhibited a broad distribution in size (Figure 3a, middle). The size distribution

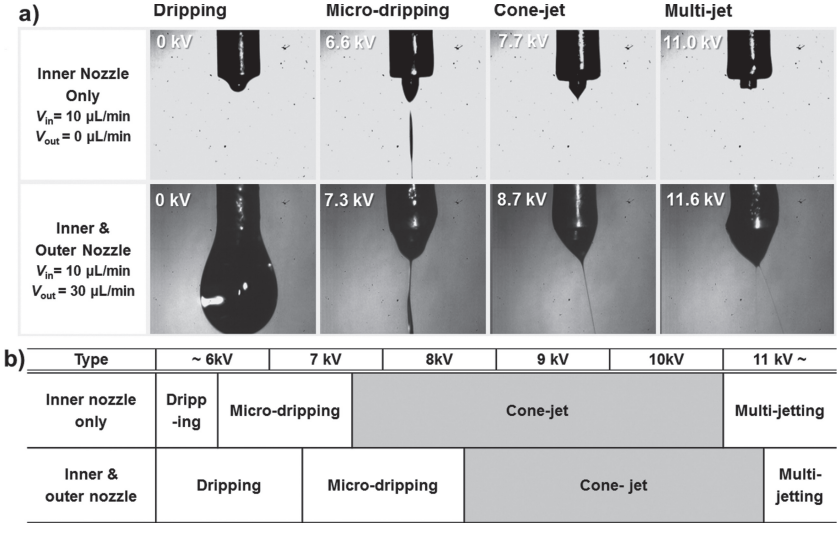

Figure 2. a) Various EHD modes with the corresponding applied voltage using an inner nozzle only (upper) and using both inner and outer nozzles (lower). b) Operating range of different modes with applied voltage.

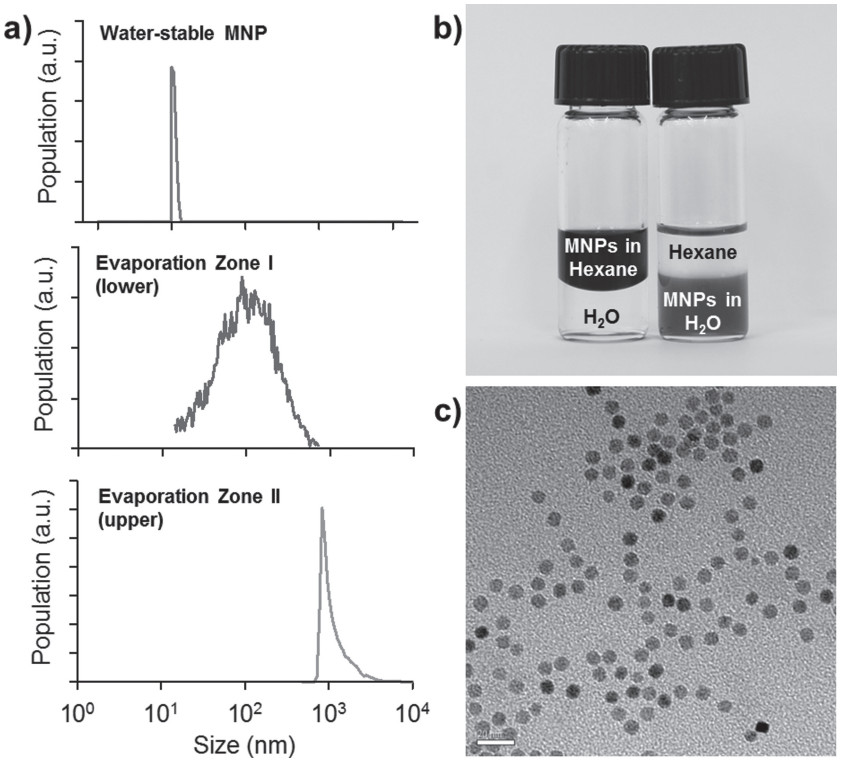

Figure 3. a) Size distributions of water-stable MNPs in an aqueous phase by DLS (upper), and atomized droplets measured by SMPS (middle) and APS (lower). b) Solubility test of water-stable MNPs in an aqueous phase. c) TEM image of water-stable MNPs.

of the fully atomized droplets was measured with a scanning mobility particle sizer (SMPS). The droplets had a total concentration of 5.32×10^3 MNPs cm^{-3}, a geometric mean diameter of 96.1 nm, and a geometric standard deviation of 2.2. After the aerosols were dropped into the aqueous phase, the MNPs were stably dispersed without any phase separation between water and hexane because of the presence of polysorbate 80 on the surface. The average size of the water-stable MNPs was 10.7 ± 0.7 nm, as measured by laser scattering. The layer of polysorbate 80 that coated the particle was approximately 1.25 nm (Figure S2 in the Supporting Information). To investigate the influence of applied voltage on particle size, we tested with various applied voltages, which resulted in various EHD modes. When the applied voltage was below 8.7 kV (microdripping mode), a bimodal size distribution of water-stable MNPs was obtained by dynamic laser scattering (DLS; Figure S3 in the Supporting Information). Two peaks were in the size range of about 10 and 100 nm. When the applied voltage was higher than 8.7 kV (cone-jet mode), unimodal size distribution was obtained. These results indicate that the coating process and the evaporation process occurred simultaneously. When polysorbate 80–MNP complexes shot out and reached an aqueous phase, hydrophilic PEG chains from polysorbate 80 had outward movement and water-soluble MNPs were prepared due to the elimination of the hydrophobic organic phase (hexane).

Coating the MNPs with a nonionic surfactant, polysorbate 80, successfully increased the solubility of the particles in an aqueous phase. The hydrophilicity of the polysorbate 80-coated MNPs was confirmed with a solubility test (Figure 3b). The oil phase of hexane floats above water due to its lower density. The MNPs coated with oleic acids were soluble only in hexane, whereas the MNPs coated with polysorbate 80 were dispersed only in the aqueous phase. The monodispersity of polysorbate 80-coated MNPs was confirmed with transmission electron microscopy (TEM, Figure 3c). The uniform-sized MNPs in the aqueous phase are advantageous for in vivo MR imaging because a heterogeneous population of nanoprobes would introduce different magnetization properties and induce complexities when recognizing and analyzing biological signals.[32] The mass ratio between the magnetic and organic components used was measured by thermogravimetric analysis (Figure S4 in the Supporting Information). The mass ratio at 600 °C was 4.8%, which indicates that organic compounds (oleic acids and polysorbate 80) were present on or within the particles. The presence of magnetic substance was verified by FTIR spectroscopy (Figure S5 in the Supporting Information). A characteristic peak for Fe–O bonding was demonstrated in the FTIR spectrum at 580 cm^{-1} in the polysorbate 80-coated MNPs. In addition, the polysorbate 80 was also confirmed by a peak at 1735 cm^{-1} due to the ester bond. Collectively, these results demonstrate that the coaxial EHDA system was able to effectively encapsulate hydrophobic MNPs with polysorbate 80 and increased the colloidal stability in an aqueous phase.

To evaluate the capabilities of the water-stable MNPs as MR imaging probes, the T_2 (spin–spin relaxation time) magnetic relaxivity coefficient ($R2$), was investigated. As shown in **Figure 4**a, T_2-weighted images gradually became darker as the concentration of water-stable MNPs was increased. $R2$, which was determined from the slope of the data in Figure 4b, was 71 mM^{-1} s^{-1}. We note that the monodispersed nature of the polysorbate 80-coated MNPs can enhance the MR signal.[32]

To further evaluate the potential of the water-stable MNPs as an MR imaging agent, we used the particles in vivo in a gastric cancer xenograft mouse model. Gastric cancer cells (10^7 MKN45 cells) were implanted in the proximal thigh of the nude mouse. When the tumor had grown to approximately 1 cm^3, the water-stable MNPs (200 μg Fe per 200 μL) were injected intravenously. The growth and heterogeneity of the tumor burden from the xenograft model was then observed with T_2-weighted MR imaging (Figure 4c, upper left). The rapid growth of the tumor induced leaks between the epithelial cells of neo-vessels produced during angiogenesis.[9] The leaky vessels enhanced the permeability of the water-stable MNPs, which then accumulated in the extravascular space of the tumor. In T_2-weighted images, dark spots are generated

NANO MICRO small

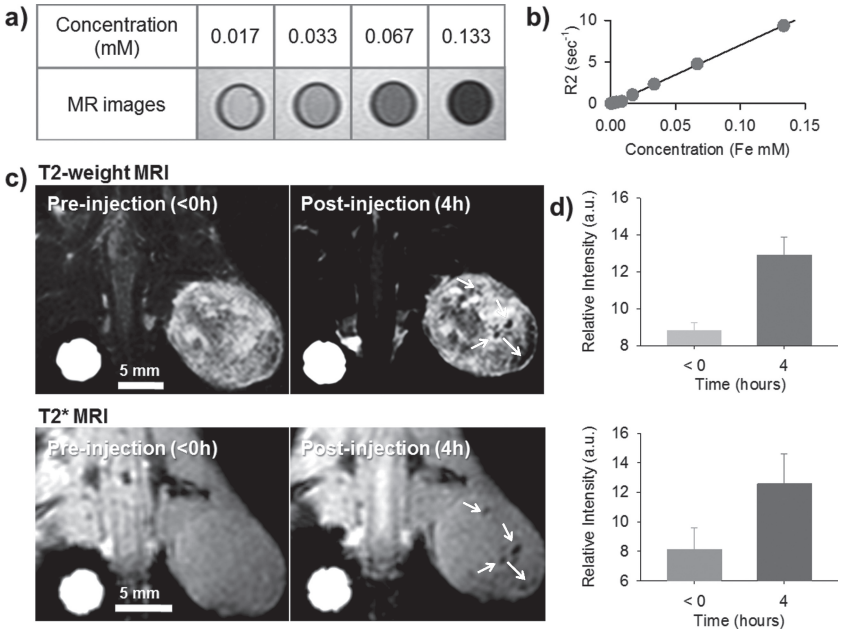

Figure 4. a) T_2-weighted MR images of water-stable MNPs in an aqueous phase at various concentrations of Fe and b) T_2 relaxivity ($R2$) graph. c) In vivo MR images (upper: T_2-weighted MR images; lower: T_2*-weighted MR images) of the xenograft mouse model implanted with MKN45 cells at the proximal thigh region of the model before (left) and after (right) injection of water-stable MNPs into the tail vein. d) Graph of the relative intensity.

by the loss of phase coherence in the processing protons due to their magnetic interaction with each other and with other fluctuating moments in the tissue (Figure 4c, upper right, red arrows). The relative intensity ($\Delta R2$) due to the magnetic components at the tumor site increased from 8.7 (<0 h) to 12.9 (4 h) (Figure 4d, upper). Furthermore, in gradient-echo T_2*-weighted MR images, signal enhancements from MNPs were even more readily detected because of the difference of magnetic susceptibility. After injection and circulation of water-stable MNPs, dark spots, due to presence of magnetic components in the tumor site, were observed (Figure 4c, lower right, red arrows) that were not apparent before injection (Figure 4c, lower left). As expected, the relative intensity in the T_2*-weighted images increased from 8.1 (<0 h) to 12.6 (4 h) (Figure 4d, lower). These results demonstrate that well-dispersed polysorbate 80-coated MNPs can be effective MR imaging probes to visualize angiogenic vessels of tumor tissue by passive accumulation.

3. Conclusion

In summary, we have developed a coaxial EHDA system for the continuous synthesis of water-stable MNPs. By modulating the flow rates through the inner and outer nozzles, we established a cone-jet mode of electrospraying for the encapsulation of MNPs with polysorbate 80. The direct fabrication of stable, PEGylated MNPs in an aqueous phase prevented their agglomeration. These water-stable MNPs had a mean diameter of 10.7 ± 0.7 nm, and exhibited great potential as an MR imaging probe in vivo. The novel coaxial EHDA system can allow continuous encapsulation and synthesis of MNPs and can be implemented for production on a large scale by a multinozzle jetting system.

4. Experimental Section

Synthesis of MNPs: Magnetic nanoparticles (MNPs, Fe_3O_4) were synthesized by thermal decomposition.[33] In detail, iron chloride (10.8 g) and sodium oleate (36.5 g) were dissolved in a mixed solvent composed of ethanol (80 mL), distilled water (60 mL), and hexane (140 mL). The resulting mixture was heated to 70 °C and reacted for 4 h. When the reaction was complete, the upper organic layer containing the iron–oleate complex was washed three times with distilled water (30 mL) in a separatory funnel. After washing, hexane was evaporated off, which resulted in an iron–oleate complex in a waxy, solid form. The synthesized iron–oleate complex (36 g) and oleic acid (5.7 g) were dissolved in 1-octadecene (200 g) at room temperature. The reaction mixture was heated to 320 °C at a constant heating rate of 3 °C min^{-1}, and then held at this temperature for 30 min. The resulting solution containing the MNPs was then cooled to room temperature, and ethanol (500 mL) was added to the solution. The MNPs were purified by centrifugation at 15 000 rpm.

Coaxial EHDA System: As shown in Figure 1, the experimental setup for the coaxial EHDA system consisted of a liquid supply system, a stirring system, a visual system, and an electrical system. The liquid supply system consisted of two syringe pumps (minimum flow rate = 16.7 pL min^{-1} for a 1 mL syringe), two feeding tubes, and a stainless steel coaxial nozzle. The coaxial nozzle consisted of a concentric outer needle (outer diameter = 1.28 mm, inner diameter = 0.84 mm) and a concentric inner needle (outer diameter = 0.5 mm, inner diameter = 0.25 mm). The inner needle was extruded 0.3 mm from the tip of the outer needle. The visual system comprised a high-speed camera (FASTCAM SA1.1, Photron) and a halogen light source (KLS-100H-RS-150, Kwangwoo Co. Ltd.) and was used to monitor the various modes of EHDA. The electrical system consisted of a high-voltage power supply (≈15 kV direct current) and two electrodes. The coaxial nozzle was used as the anode, and a plate-type electrode located 3 cm below the tip of the nozzle was used as the ground electrode. The stirring system was located below the ground electrode to prevent aggregation between MNPs in the DI water.

Characterization: The viscosity and electrical conductivity of the solutions (MNPs in hexane and polysorbate 80) were measured using a vibration viscometer (SV-10, AND, Japan) and conductivity meter (F-54, Horiba, Japan), respectively. Surface tension was measured by the well-known Du Nouy ring method. The size distributions of the MNPs dispersed in an organic phase and in an aqueous phase were analyzed by laser scattering (ELS-Z, Otska Electronics). The morphology and size of the MNPs in the aqueous phase were measured with a transmission electron microscope (JEM-1011, JEOL Ltd.). The system used to measure the size of aerosols containing MNPs is shown in Figure S1. The size distribution was measured by an aerodynamic particle sizer (APS, TSI model 3021) and a scanning mobility particle sizer (SMPS, TSI model 3936), which consisted of a differential mobility analyzer

(TSI model 3081) and a condensation particle counter (TSI model 3775). Sampling points were located near the break-up point for the APS and near the ground plate for the SMPS.

In vivo MR Imaging: All animal experiments were conducted with the approval of the Association for Assessment and Accreditation of Laboratory Animal Care International. MKN-45 gastric cancer cell line was obtained from the American Type Culture Collection. To establish the xenograft mouse model for gastric cancer, MKN-45 cells (10^7 cells) were implanted into the proximal thigh of male mice (6-week-old BALB/c nude mice). At predetermined time points, the lengths of the minor axis ($2a$) and the major axis ($2b$) of tumors were measured using calipers. Tumor volume was then calculated using the formula for a prolate spheroid: $(4/3)p \times a^2\ b$. When the tumor size reached approximately 500 mm^3, water-soluble MNPs were injected intravenously into the tail vein. In vivo MR imaging experiments were performed with a 3T clinical MR imaging instrument with a micro-47 surface coil (Philips Medical Systems). The T_2-weighted MR images of nude mice injected with the prepared materials at 3T were acquired using the following parameters at room temperature: $T_R = 4000$ ms even echo space, number of acquisitions = 1, point resolution of 312 × 312 mm, section thickness of 0.6 mm, and $T_E = 60$ ms.

Supporting Information

Supporting Information is available from the Wiley Online Library or from the author.

Acknowledgements

This study was supported by the Global Frontier R&D Program on Center for Multiscale Energy System, Basic Science Research Program through the National Research Foundation of Korea (NRF) funded by the Ministry of Education, Science, and Technology (2010-0023202), and a grant from the National R&D Program for Cancer Control, Ministry for Health and Welfare, Republic of Korea (1020390).

[1] Q. A. Pankhurst, J. Connolly, S. K. Jones, J. Dobson, *J. Phys. D: Appl. Phys.* **2003**, *36*, R167–R181.
[2] S. Mornet, S. Vasseur, F. Grasset, E. Duguet, *J. Mater. Chem.* **2004**, *14*, 2161–2175.
[3] Y. W. Jun, Y. M. Huh, J. S. Choi, J. H. Lee, H. T. Song, S. Kim, S. Yoon, K. S. Kim, J. S. Shin, J. S. Suh, J. Cheon, *J. Am. Chem. Soc.* **2005**, *127*, 5732–5733.
[4] K. L. Hultman, A. J. Raffo, A. L. Grzenda, P. E. Harris, T. R. Brown, S. O'Brien, *ACS Nano* **2008**, *2*, 477–484.
[5] C. C. Berry, A. S. G. Curtis, *J. Phys. D: Appl. Phys.* **2003**, *36*, R198–R206.
[6] S. M. Moghimi, A. C. Hunter, J. C. Murray, *Pharmacol. Rev.* **2001**, *53*, 283–318.
[7] J. Xie, C. Xu, N. Kohler, Y. Hou, S. Sun, *Adv. Mater.* **2007**, *19*, 3163–3166.
[8] J. H. Lee, Y. M. Huh, Y. W. Jun, J. W. Seo, J. T. Jang, H. T. Song, S. Kim, E. J. Cho, H. G. Yoon, J. S. Suh, J. Cheon, *Nat. Med.* **2007**, *13*, 95–99.
[9] J. Yang, T.-I. Lee, J. Lee, E.-K. Lim, W. Hyung, C.-H. Lee, Y. J. Song, J.-S. Suh, H.-G. Yoon, Y.-M. Huh, S. Haam, *Chem. Mater.* **2007**, *19*, 3870–3876.
[10] J. Yang, C.-H. Lee, H.-J. Ko, J.-S. Suh, H.-G. Yoon, K. Lee, Y.-M. Huh, S. Haam, *Angew. Chem. Int. Ed.* **2007**, *46*, 8836–8839.
[11] E. Amstad, T. Gillich, I. Bilecka, M. Textor, E. Reimhult, *Nano Lett.* **2009**, *9*, 4042–4048.
[12] H. Lee, E. Lee, D. K. Kim, N. K. Jang, Y. Y. Jeong, S. Jon, *J. Am. Chem. Soc.* **2006**, *128*, 7383–7389.
[13] U. I. Tromsdorf, O. T. Bruns, S. C. Salmen, U. Beisiegel, H. Weller, *Nano Lett.* **2009**, *9*, 4434–4440.
[14] C. Sun, K. Du, C. Fang, N. Bhattarai, O. Veiseh, F. Kievit, Z. Stephen, D. Lee, R. G. Ellenbogen, B. Ratner, M. Zhang, *ACS Nano* **2010**, *4*, 2402–2410.
[15] Q. L. Fan, K. G. Neoh, E. T. Kang, B. Shuter, S. C. Wang, *Biomaterials* **2007**, *28*, 5426–5436.
[16] E. Amstad, S. Zurcher, A. Mashaghi, J. Y. Wong, M. Textor, E. Reimhult, *Small* **2009**, *5*, 1334–1342.
[17] D. Liu, W. Wu, J. Ling, S. Wen, N. Gu, X. Zhang, *Adv. Funct. Mater.* **2011**, *21*, 1498–1504.
[18] S. J. Sofia, V. Premnath, E. W. Merrill, *Macromolecules* **1998**, *31*, 5059–5070.
[19] I. Szleifer, *Biophys. J.* **1997**, *72*, 595–612.
[20] R. Abu Mukh-Qasem, A. Gedanken, *J. Colloid Interface Sci.* **2005**, *284*, 489–494.
[21] A. Barrero, I. G. Loscertales, *Annu. Rev. Fluid Mech.* **2007**, *39*, 89–106.
[22] I. G. Loscertales, A. Barrero, I. Guerrero, R. Cortijo, M. Marquez, A. M. Gañán-Calvo, *Science* **2002**, *295*, 1695–1698.
[23] Y. K. Hwang, U. Jeong, E. C. Cho, *Langmuir* **2008**, *24*, 2446–2451.
[24] A. Gomez, D. Bingham, L. De Juan, K. Tang, *J. Aerosol Sci.* **1998**, *29*, 561–574.
[25] X. Li, J. Huang, Z. Ahmad, M. Edirisinghe, *Biomed. Mater. Eng.* **2007**, *17*, 335–346.
[26] K. Balasubramanian, S. N. Jayasinghe, M. J. Edirisinghe, *Int. J. Appl. Ceram. Technol.* **2006**, *3*, 55–60.
[27] M. Enayati, Z. Ahmad, E. Stride, M. Edirisinghe, *J. R. Soc. Interface* **2010**, *7*, 667–675.
[28] R. Pareta, M. J. Edirisinghe, *J. R. Soc. Interface* **2006**, *3*, 573–582.
[29] J. E. Díaz Gómez, A. G. Marín, M. Marquez, A. Barrero, I. G. Loscertales, *Biotechnol. J.* **2006**, *1*, 963–968.
[30] Á. G. Marín, I. G. Loscertales, M. Márquez, A. Barrero, *Phys. Rev. Lett.* **2007**, *98*, 014502.
[31] Z. Ahmad, H. B. Zhang, U. Farook, M. Edirisinghe, E. Stride, P. Colombo, *J. R. Soc. Interface* **2008**, *5*, 1255–1261.
[32] A. K. Gupta, M. Gupta, *Biomaterials* **2005**, *26*, 3995–4021.
[33] P. R. Fitzgerald, M. E. Mansfield, *J. Protozool.* **1973**, *20*, 121–126.

Received: July 4, 2012
Revised: September 25, 2012
Published online: February 1, 2013

